Title

Quantitative multiparametric MRI in uveal melanoma: increased tumor permeability may predict monosomy 3

Journal

Neuroradiology, 57(8)

ISSN

0028-3940

Authors

Kamrava, M
Sepahdari, AR
Leu, K
et al.

Publication Date

2015-08-31

DOI

10.1007/s00234-015-1546-0

Peer reviewed

Neuroradiology (2015) 57:833–840
DOI 10.1007/s00234-015-1546-0

HEAD AND NECK RADIOLOGY

Quantitative multiparametric MRI in uveal melanoma: increased tumor permeability may predict monosomy 3

Mitchell Kamrava[1] · Ali R Sepahdari[2] · Kevin Leu[2] · Pin-Chieh Wang[1] · Kristofer Roberts[1] · D. Jeffrey Demanes[1] · Tara McCannel[3] · Benjamin M. Ellingson[2]

Received: 26 January 2015 / Accepted: 19 May 2015 / Published online: 29 May 2015

Abstract
Introduction Uveal melanoma is a rare intraocular tumor with heterogeneous biological behavior, and additional noninvasive markers that may predict outcome are needed. Diffusion- and perfusion-weighted imaging may prove useful but have previously been limited in their ability to evaluate ocular tumors. Our purpose was to show the feasibility and potential value of a multiparametric (mp-) MRI protocol employing state of the art diffusion- and perfusion-weighted imaging techniques.
Methods Sixteen patients with uveal melanoma were imaged with mp-MRI. Multishot readout-segmented echoplanar diffusion-weighted imaging, quantitative dynamic contrast-enhanced (DCE) MR perfusion imaging, and anatomic sequences were obtained. Regions of interest (ROIs) were drawn around tumors for calculation of apparent diffusion coefficient (ADC) and perfusion metrics (K^{trans}, v_e, k_{ep}, and v_p). A generalized linear fit model was used to compare various MRI values with the American Joint Commission on Cancer (AJCC) tumor group and monosomy 3 status with significance set at $P<0.05$.
Results mp-MRI was performed successfully in all cases. MRI tumor height (mean [standard deviation]) was 6.5 mm (3.0). ROI volume was 278 mm^3 (222). ADC was 1.07 (0.27)×10–3 mm^2/s. DCE metrics were K^{trans} 0.085/min (0.063), v_e 0.060 (0.052), k_{ep} 1.20/min (0.32), and v_p 1.48 % (0.82). Patients with >33 % monosomy 3 had higher K^{trans} and higher v_e values than those with disomy 3 or ≤33 % monosomy ($P<0.01$). There were no significant differences between ADC ($P=0.07$), k_{ep} ($P=0.37$), and v_p with respect to monosomy 3.
Conclusion mp-MRI for ocular tumor imaging using multishot EPI DWI and quantitative DCE perfusion is technically feasible. mp-MRI may help predict monosomy 3 in uveal melanoma.

Keywords Uveal melanoma · Multiparametric MRI · Diffusion-weighted imaging · MR perfusion imaging · Personalized medicine

List of abbreviations

DWI	Diffusion-weighted imaging
DCE	Dynamic contrast-enhanced
ADC	Apparent diffusion coefficient
CISS	Constructive interference in steady state
EPI	Echoplanar imaging

Introduction

Uveal melanoma is a rare tumor, with an annual incidence of approximately six per million and overall 5-year mortality reported at 16–53 %. It is both biologically and spatially heterogeneous

Mitchell Kamrava and Ali R Sepahdari contributed equally to this work.

✉ Ali R Sepahdari
ali.sepahdari@gmail.com

[1] Department of Radiation Oncology, University of California Los Angeles, 200 Medical Plaza, Ste B265, Los Angeles, CA 90095, USA

[2] Department of Radiological Sciences, University of California Los Angeles, Los Angeles, CA, USA

[3] Department of Ophthalmology, University of California Los Angeles, Los Angeles, CA, USA

[1]. Though fine-needle aspiration biopsy can be used to identify prognostic markers such as monosomy 3 [2], noninvasive markers to stratify risk for metastasis are lacking.

To date, magnetic resonance imaging (MRI) of uveal melanoma has mostly been limited to describing features such as T2 signal, T1 signal, and contrast enhancement. Perfusion-weighted MRI of uveal melanoma has focused on describing the shape of the time-intensity curve; previously described techniques have lacked sufficient temporal resolution to determine quantitative pharmacokinetic information [3]. Diffusion-weighted imaging (DWI) of uveal melanoma has been performed [4, 5] but has only been used to distinguish uveal melanoma from surrounding retinal detachment, rather than to further characterize the biology of the tumor. DWI has notably been limited by magnetic susceptibility artifacts, precluding characterization of small tumors and degrading image quality overall [5]. Ideally, advanced MRI including DWI and perfusion-weighted imaging may be used to subcategorize uveal melanoma tumors by providing quantitative information for multiple vascular parameters, including permeability, washout rate, and interstitial space per unit volume, as well as estimates of the apparent diffusion coefficient (ADC), which is a surrogate marker for cellularity. Correlating the diffusion and perfusion characteristics with known prognostic markers, such as monosomy 3, may ultimately expand the role of advanced imaging in uveal melanoma from diagnostic to prognostic.

The purpose of this study is to show the feasibility of a multiparametric MRI protocol for ocular melanoma imaging, using quantitative dynamic contrast-enhanced (DCE) MR-perfusion imaging employing echoplanar imaging (EPI) T1-weighted imaging and DWI using a multishot EPI sequence that reduces susceptibility artifact. A subsequent exploratory analysis of mp-MRI characteristics with monosomy 3 status was also evaluated.

Methods

Subjects

This Health Insurance Portability and Accountability Act complaint, Institutional-Review-Board-approved study was performed with a waiver of informed consent. Consecutive patients imaged with a multiparametric ocular tumor MRI protocol were prospectively studied. Sixteen subjects, 5 female and 11 male, with primary uveal melanoma were imaged over a 33-month period. The subjects had an average age of 59 years (range 27–77).

MRI

Detailed parameters of each sequence can be found in Table 1. A 1.5-T MR scanner was used for all image acquisition (Avanto; Siemens Healthcare AG, Erlangen, Germany). Patients were instructed not to wear eye makeup and to keep their eyes closed during scanning. Pre-contrast sagittal and axial T1-weighted spin-echo, axial heavily T2-weighted three-dimensional constructive interference in the steady state (CISS) sequences, and axial multishot EPI DWI were obtained through the orbits. The CISS images were reformatted in oblique planes in order to obtain tumor measurements. DWI was performed with a multishot (nine shots), spin-echo, EPI sequence with $b=0$ and 800 s/mm^2 (RESOLVE). An ADC map was generated from the $b=0$ and 800 s/mm^2 data sets. Tumors were manually contoured on the ADC maps on multiple slices using the OsiriX viewer for Mac [6], and an average ADC was obtained for each tumor based on the contoured volume. Following DCE-MRI acquisition (below), a post-contrast axial T1-weighted spin-echo sequence was obtained.

DCE-MRI

Initially, fast low-angle shot (FLASH) images with flip angles of 2°, 5°, 15°, 20°, and 25° were acquired in four matched slices through the center of the tumor. Dynamic FLASH images with a flip angle of 25° were then acquired at a 6-s temporal frame rate during a 5 cm^3/s bolus injection of 0.1 mmol/kg Gd-diethylene triamine pentaacetic acid (DTPA), followed by a 20-cc injection of isotonic saline, with a 30-s baseline. Seventy time points were obtained over the 7-min acquisition time.

DCE-MRI post-processing consisted of first using the Ernst angle [4] equation to fit T1 to the multiple flip angle data on a voxel-wise basis using the nonlinear least squares regression algorithm (*3dNLfim*) in AFNI (*Analysis of Functional Neuroimages Software Package*; *NIH/NIMH*; http://afni.nimh.nih.gov/afni), using in-house MATLAB scripts. The DCE-MRI dynamic time series was then converted to a dynamic series reflecting the change in T1 with respect to the established baseline ($\Delta R1(t)$). A dynamic concentration versus time series ($C(t)$) was then created from the dynamic T1 time series, assuming a relaxivity of Gd-DTPA of 4.5/mM s [7]. All DCE-MRI images for each subject and scan session were registered to the baseline T1-weighted post-contrast image using a 12-degree-of-freedom affine transformation and a mutual information cost function to account for motion between each image sequence (FMRIB Software Library (FSL); FMRIB, Oxford, UK; http://www.fmrib.ox.ac.uk/fsl/). If required, manual alignment was subsequently performed (tkregister2, Freesurfer; surfer.nmr.mgh.harvard.edu; Massachusetts General Hospital, Harvard Medical School).

Manual regions of interest (ROIs) were drawn within both internal carotid arteries (ICAs), which were used as the

Table 1 Detailed MRI pulse sequence information

	Axial T1 (pre- and post-contrast)	Sagittal T1	Axial 3D-CISS	Multishot DWI (RESOLVE)	DCE-MRI[a]
TR/TE (ms)	400/7.8	400/7.8	5.42/2.42	2500/72	27/2.87
FOV (mm)	157×160	230×130	135×180	229×229	119×239
Matrix	256×214	320×224	256×192	224×224	448×202
Slick thickness/gap (mm)	3/0	5/1.5	0.7/0	2.5/0	3/0
Flip angle	90	90	70	90	25
NEX	2	1	1	3	1

TR repetition time, *TE* echo time, *FOV* field of view, *NEX* number of excitations, *CISS* constructive interference in steady state, *DCE* dynamic contrast-enhanced

[a] DCE-MRI was performed with parallel acceleration factor of 2 and 6/8 partial Fourier acquisition

patient-specific arterial input function (AIF) as previously described [8]. Nonlinear least squares regression was used to fit the dynamic concentration versus time curves $C(t)$ to the standard three-parameter Tofts model [9, 10], on a voxel-by-voxel basis to extract parameters of interest: K^{trans} (vascular permeability in /min), v_e (interstitial space per unit volume of tissue [unitless]), k_{ep} (flux rate constant between the extravascular and extracellular space and blood plasma), and v_p (fractional plasma volume). Voxels with a significant fit to model parameters (i.e., $r^2>0.7$ and a level of significance $P<0.05$) were retained for analysis. ROIs were then defined on post-contrast, T1-weighted images for the region of contrast-enhancing solid tumor and normal-appearing white matter (NAWM) in the pons (Fig. 1).

Treatments

Patients underwent intraoperative transscleral fine-needle biopsy aspiration during plaque brachytherapy. Biopsy specimens were processed for cytopathologic and cytogenetic analysis. Chromosome 3 status was evaluated at the University of California Los Angeles Clinical Cytogenetics Laboratory, a standardized CLIA-approved laboratory with a cytogeneticist experienced in interpreting and reporting fluorescent in situ hybridization (FISH) results for uveal melanoma. Cells collected for cytogenetic analysis were gently spun down in a sterile conical tube and resuspended in Roswell Park Memorial Institute 1640 (RPMI-1640) media (Gibco [Invitrogen], Carlsbad, CA, USA) supplemented with antibiotics and 10 % bovine serum (Irvine Scientific, Santa Ana, CA, USA). The cultures were prepared according to standard protocols. For FISH analysis, a directly labeled centromeric probe specific for chromosome 3, CEP-3 Spectrum Orange (Vysis, Downers Grove, IL, USA), was used to assess monosomy or disomy. This probe was hybridized to fixed cultured cells following the manufacturer's protocol (Abbott-Vysis, Des Plaines, IL, USA). Hybridization signals were counted by hand in nonoverlapping nuclei of cells under a fluorescence microscope (Axiophot, Carl Zeiss Mikroskopie, Jena, Germany) equipped with a triple filter (diamino-2-phenylindole dihydrochlordie/fluorescein isothiocyanate/Texas Red). When any cells were found to contain only one copy of chromosome 3, the sample was considered positive for monosomy 3.

Statistical analysis

A generalized linear fit model was used to compare various MRI values with the American Joint Commission on Cancer (AJCC) tumor group and monosomy 3 status. In the analysis of monosomy 3 status, a cutoff of 33 % was employed based on published data demonstrating its significance in metastasis-free survival [2]. $P<0.05$ was considered significant.

Results

A total of 16 patients with primary uveal melanoma underwent mp-MR (Table 2, online only). The average±standard deviation (SD) MRI tumor height was 6.5±3.0 mm. ROIs were identified and contoured for each patient with the average±SD volume being 278±222 mm^3. Mean±SD ADC for all patients was $1.13\pm0.36\times10^{-3}$ mm^2/s. The mean±SD DCE metrics of K^{trans}, v_e, k_{ep}, and v_p were 0.085±0.063/min, 0.060±0.052, 1.20±0.32/min, and 1.48±0.82 %, respectively (Table 3, online only). NAWM was used as an internal control to help confirm measurement validity. K^{trans} value for NAWM was consistent with published values [11].

A comparison of AJCC stage and the mp-MRI parameters ADC, K^{trans}, v_e, k_{ep}, and v_p was performed to investigate any correlations. The distribution of AJCC groups 1, 2, 3, and 4 was three, six, six, and one patients, respectively. There were no significant correlations between mp-MRI parameters and AJCC group.

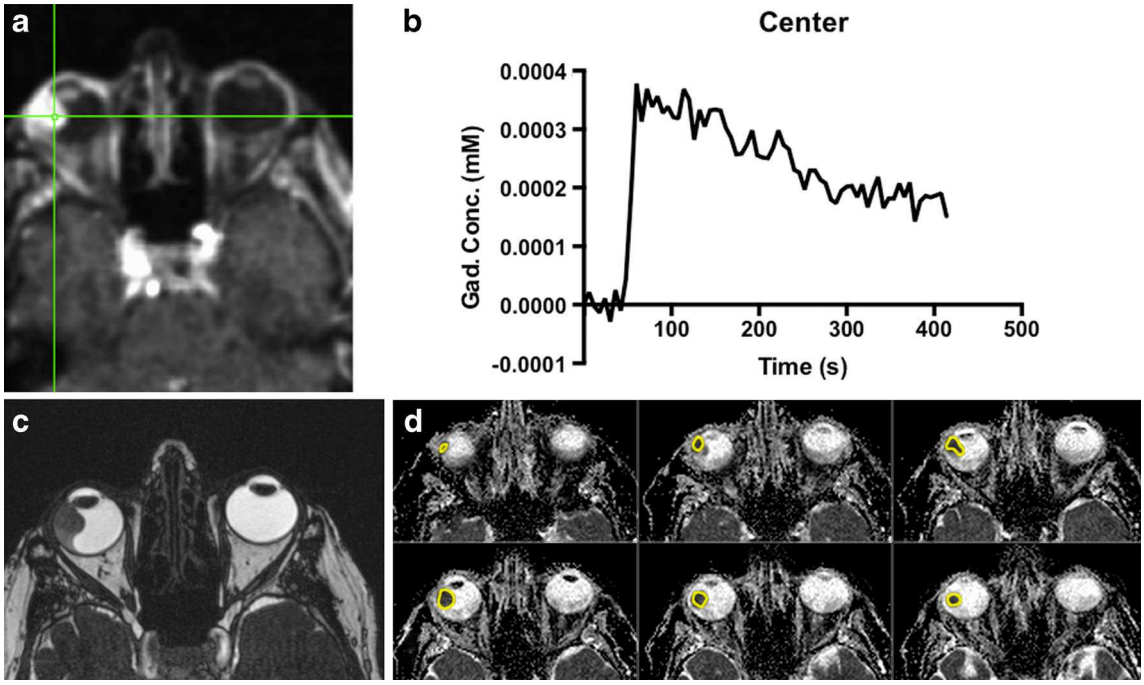

Fig. 1 Representative example of multiparametric MRI. Right ocular melanoma, exhibiting monosomy 3. **a** Average intensity projection image from dynamic MR perfusion time series, with a sample voxel placement (note that the entire lesion was contoured for data analysis). **b** Time-intensity curve from the voxel sampled in **a** shows rapid wash-in of contrast, consistent with elevated K^{trans}. **c** Axial constructive interference in the steady-state MR image shows sharp demarcation between hypointense tumor anteriorly, hyperintense vitreous humor, and intermediate signal fluid beneath a detached retina. These images were reformatted in oblique planes to obtain tumor measurements. **d** Axial apparent diffusion coefficient images from multishot EPI diffusion-weighted imaging visualize the tumor well, without anatomic distortions. The tumor is readily contoured on multiple contiguous slices

Signal-to-noise ratio (SNR) measurements were obtained from six representative AJCC group 1, 2, and 3 tumors. SNR was calculated as the mean of the tumor at baseline minus the mean of the background divided by the standard deviation of the baseline.

Table 2 Patient characteristics

Patient no.	Age at diagnosis (years)	MRI tumor height (mm)	MRI basal dimensions (mm)
1	66	9	8.9×8.5
2	72	2	15×8
3	68	2	6.5×6.5
4	74	2	6.1×7.0
5	57	8	15.1×12.8
6	77	7.5	8.3×9.3
7	43	7	8.2×9.1
8	51	9.5	15.5×11.9
9	37	9	12.8×11.1
10	73	4.5	12.3×11.9
11	57	4.7	15.7×14.3
12	58	3.5	9×9
13	67	11	14×11
14	54	9	15×18
15	57	7.6	20.2×19.7
16	61	8.1	15.4×17.5

The AJCC group 1 tumors had a mean SNR of 4.4. Group 2 tumors had a mean SNR of 5.0. Group 3 tumors had a mean SNR of 7.5. Lower SNR in small tumors was reflected in visual analysis of the time-intensity curves (TICs), which showed wider point-to-point variations compared to TICs of larger tumors (Fig. 2).

Tumors were evaluated with fine-needle aspiration performed at the time of plaque placement. Fine-needle aspiration was performed in all patients, but sufficient material for diagnosis was obtained in only 12 of 16 cases. Of these, 7/12 did not have monosomy 3, 4/12 had monosomy 3 in >33 % of the examined cells, and 1/12 had monosomy 3 in ≤33 % of the examined cells. There was a significant correlation between K^{trans} and monosomy 3 >33 % (Fig. 3) and between v_e and monosomy 3 >33 % ($P<0.01$). Patients with >33 % monosomy 3 had higher K^{trans} than those with disomy 3 or ≤33 % monosomy (0.145 versus 0.061/min, $P<0.01$). No significant differences were found between k_{ep} ($P=0.37$) values and monosomy 3 status. There was a nonsignificant trend toward lower ADC in monosomy 3 (0.80±0.07) than in disomy 3 or ≤33 % monosomy 3 (1.03±0.20), with $P=0.07$. There was also a nonsignificant trend toward higher v_p in monosomy 3

Table 3 Multiparametric MRI metrics for each tumor

Patient no.	Monosomy 3 status (%)	ROI volume (mm^3)	ADC mean tumor (10^{-3} mm^2/s)	K^{trans} (/min)	v_e	k_{ep} (/min)	v_p (%)
1	90	548	0.76	0.189	0.097	0.97	1.53
2	0	159	1.21	0.011	0.011	1.01	0.45
3	Unknown	356	1.47	0.018	0.015	1.13	0.94
4	Unknown	259	1.35	0.015	0.015	0.88	0.68
5	0	103	0.75	0.092	0.059	1.38	1.29
6	0	99	1.05	0.130	0.069	1.86	1.67
7	Unknown	58	1.31	0.211	0.224	0.52	0.87
8	62	302	0.80	0.104	0.063	1.55	1.54
9	23	125	1.13	0.057	0.050	0.94	0.53
10	0	35	0.82	0.033	0.025	1.21	0.87
11	0	108	1.35	0.150	0.093	1.44	2.58
12	0	92	1.05	0.042	0.034	1.11	0.63
13	97	553	0.75	0.027	0.023	1.10	2.63
14	Unknown	381	1.52	0.064	0.045	1.27	1.01
15	0	833	0.92	0.076	0.049	1.21	1.46
16	70	485	0.91	0.137	0.082	1.60	2.69
Average (std dev)		281 (229)	1.13 (0.36)	0.085 (0.063)	0.060 (0.052)	1.20 (0.32)	1.48 (0.82)
≤33 % monosomy	361 (198)	1.03 (0.20)	0.061 (0.039)*	0.041 (0.020)*	1.25 (0.28)	1.19 (0.74)	
>33 % monosomy	254 (240)	0.80 (0.07)	0.145 (0.035)*	0.084 (0.015)*	1.39 (0.29)	2.08 (0.67)	

K^{trans}, v_e, k_{ep}, and v_p median values for each tumor are reported

*$P<0.01$

(2.10±0.67 %) compared to disomy 3 or ≤33 % monosomy 3 (1.19±0.74 %), with $P=0.07$.

Discussion

We report the technical feasibility of an mp-MRI protocol for uveal melanoma imaging that includes DWI, DCE-MRI, and volumetric heavily T2-weighted sequences. This technique revealed information on tumor volume, apparent diffusion coefficient, and multiple perfusion parameters including enhancement pattern, permeability, washout rate, and fractional plasma volume. Each of these components was successfully performed, with high technical image quality, even in small lesions.

The broad range of tumor ADCs and tumor perfusion values that we observed were likely reflective of biological heterogeneity between tumors. The statistically significant associations between K^{trans} and monosomy 3 and between v_e and monosomy 3 are hypothesis generating and will require further validation as possible noninvasive biomarkers.

The sequences used present a novel technique that advances previously used protocols. Recent studies have characterized retinoblastoma and melanoma tumors with single-shot spin-echo echoplanar DWI [4, 5] and have characterized retinoblastoma with turbo spin-echo DWI [12], but each of these techniques has limitations. Single-shot spin-echo EPI DWI is limited by warping artifacts, whereas turbo spin-echo DWI is limited by poor SNR relative to the acquisition time. The RESOLVE DWI sequence employed here balances artifact reduction and SNR maximization.

Previous investigators have studied uveal melanoma with spin-echo T1 DCE-MRI techniques [3], whose lower temporal resolution produces less accurate time-enhancement curves and precludes determination of advanced quantitative markers such as K^{trans}. CT perfusion has been used to study ocular melanoma [13]. Although CT is more widely available, multiparametric MRI is superior as it (1) provides information on tumor cellularity with ADC, (2) achieves superior contrast compared to CT, and (3) avoids heavy radiation exposure to the lens of the eye. Volumetric heavily T2-weighted sequences, as employed here, effectively determine tumor volume in ocular melanoma [14] and may also assist in designing brachytherapy plaques and calculating tumor dosimetry.

In addition to showing the feasibility of mp-MRI for ocular tumor imaging, we also obtained quantitative data on diffusion and perfusion in uveal melanoma, for which current data are limited. The ADC values that we measured are similar to other reports in the literature. One study on 40 ocular melanoma patients from Erg-Eigner et al. found mean ADC values of 0.891×10^{-3} mm^2/s [4]. Their study included patients imaged

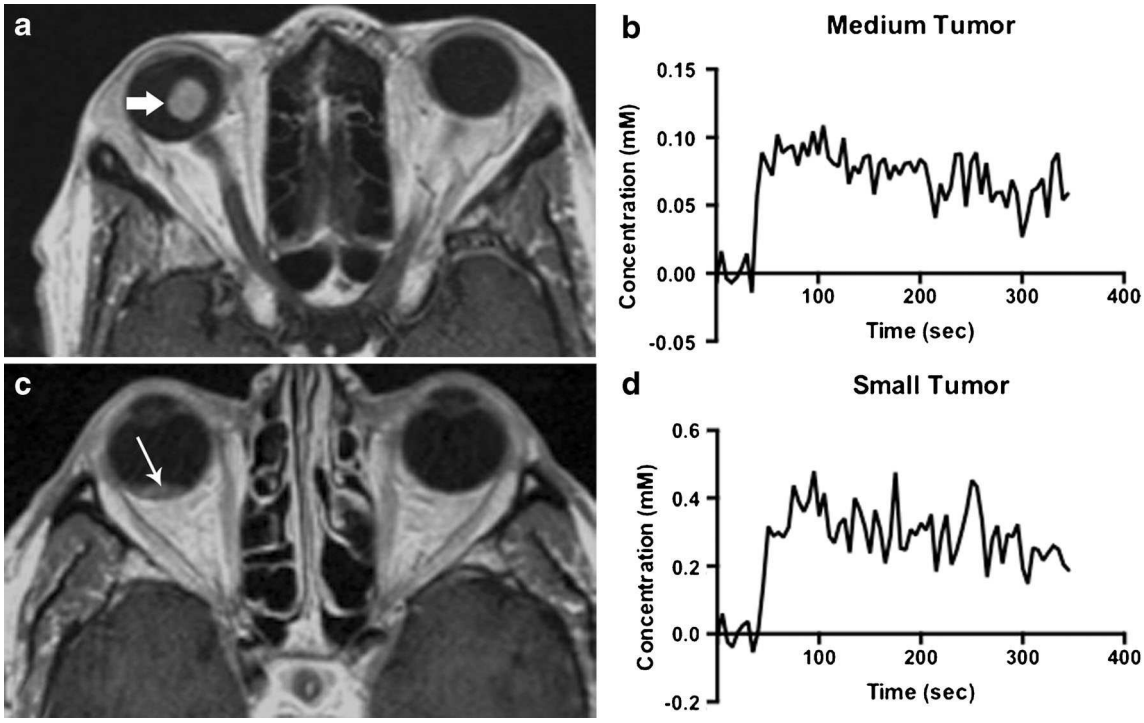

Fig. 2 Medium and small-size tumors imaged with multiparametric MRI. Time-intensity curves (TICs) are shown for medium and small-size tumors. **a** Contrast-enhanced T1-weighted image shows a medium size, AJCC group 2 tumor. **b** TIC for the tumor in **a** shows a brisk signal increase following contrast bolus infusion. **c** Contrast-enhanced T1-weighted image shows a small, plaque-like AJCC group 1 tumor. **d** TIC for the tumor in **c** shows a similarly brisk signal increase as for the medium-size tumor but with more point-to-point variation along the curve, possibly related to eye motion

on both 1.5 and 3-T machines and the mean tumor height was 14 mm. This is somewhat different from our cohort where all patients were imaged on a 1.5-T scanner and the average tumor height was 6.6 mm. Sepahdari et al. reported a study of five patients with ocular melanoma with mean ADC values of 1.18×10^{-3} mm^2/s and 6.6-mm average tumor thickness [4]. Finally, a recent study from Foti et al. noted a mean ADC value of 1.04×10^{-3} mm^2/s in 10 subjects [15]. It is not clear whether the lower ADC values in the study from Erb-Eigner et al. represent differences in imaging technique and/or whether larger tumors are more restricted. Although Sepahdari et al. noted that smaller ocular tumors show higher ADC, likely due to partial volume averaging effect [5], we did not see a significant trend in ADC values with tumor height in our patient cohort. This was likely a result of the higher resolution MRI technique used here, which resulted in accurate characterization of even the smallest lesions. While we believe that the ADC values for ocular melanoma are lower than normal surrounding tissues, we did not find that ADC is always well below 1.0×10^{-3} mm^2/s, as was suggested by Erb-Eigner et al.

Perfusion data in uveal melanoma are more limited than diffusion data. Yuan et al. reported on DCE parameters in 16 malignant orbital masses [16], of which 4 were ocular melanoma. All four cases had a washout pattern with a rapid increase in slope and final intensity lower than 90 % of the peak. Other parameters like maximum enhancement ratio, time of peak enhancement, and maximum rise of slope provided high sensitivity for identifying malignant versus benign lesions. Although their findings suggest that malignant ocular tumors have unique perfusion characteristics compared to benign lesions, our study provides unique quantitative data and also identifies biological heterogeneity within ocular melanoma.

mp-MRI revealed a significant correlation between K^{trans} and percent of monosomy 3≥33 %. In general, determination of monosomy 3 status is an extremely important prognostic marker in uveal melanoma as published series have demonstrated 5-year survival rates of 30 % for monosomy 3-positive patients, while those with nonmonosomy 3 ocular melanoma carry 5-year survival rates of nearly 100 % [17]. Our cutoff of stratifying patients by monosomy 3 ≥33 % is based on literature showing that patients with tumors having more than 33 % of cells positive for monosomy 3 have a poorer prognosis than those with tumors with lower percentages [2]. Differences in angiogenesis could explain the observed correlation of K^{trans} and monosomy 3. Vascular endothelial growth factor and hypoxia-inducible factor 1α have both been detected in uveal melanoma; however, conflicting data exist regarding the relationship between their expression levels, rate of metastasis, and patient survival [18–20]. Furthermore, neither VEGF nor HIF-1α levels have been definitely correlated with monosomy 3 status.

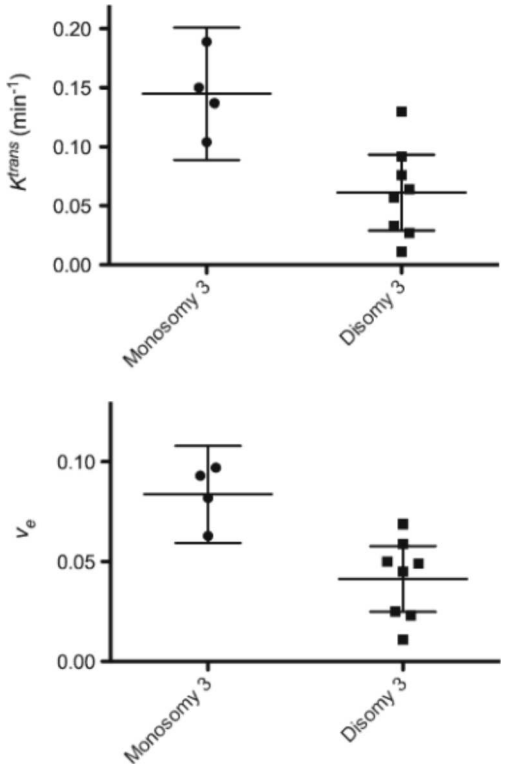

Fig. 3 Scatter plot of K^{trans} and v_e, segregated by monosomy 3 status. Tumors with monosomy 3 showed elevated K^{trans} compared to tumors with disomy 3 ($P<0.01$), indicative of increased permeability. Tumors with monosomy 3 also showed increased interstitial space per unit volume ($P<0.01$). Mean and 95 % confidence intervals are marked

Due to the highly technical nature of perfusion post-processing, discussion of certain assumptions and limitations is necessary. The Tofts model is a method that enables analysis of the blood vessels generated by a tumor via a nonlinear fit to a two-compartment pharmacokinetic model, though the model has a few limitations related to physiological interpretability of the yielded parameters. According to Sourbron et al. [21], the extended Tofts model, as used in this study, yields accurate values to tissues that are either weakly vascularized (small blood volume) or highly perfused. In general, ocular melanomas are highly vascularized but have small blood volumes. It is conceivable that the physiological interpretation of the values produced by the Tofts model could be unclear for larger tumors, as the blood volume increases. Additionally, K^{trans} itself may have multiple interpretations. Under high-permeability conditions [22, 23], K^{trans} tends to represent flow, whereas it represents permeability-surface area product under high-flow conditions. Finally, it represents the product of extraction fraction and flow under mixed conditions. While we believe that the ocular melanoma tumors represent a condition of mixed flow- and permeability-limited conditions, the degree of mixing could influence the interpretability of K^{trans}.

Several additional limitations were present. The duration of the perfusion acquisition affects calculations of v_e, k_{ep}, and v_p. The 7-min DCE acquisition may be inadequate to acquire reliable data for these late curve phenomena. Eye motion and associated misregistration artifacts may have compromised evaluation of the smallest tumors. Finally, the small size of these tumors and limited SNR limit the usefulness of colorized post-processed perfusion maps and voxel-wise or histogram analysis of quantitative parameters of perfusion, i.e., it is difficult to assess the heterogeneity of such small tumors due to the superimposed heterogeneity related to background noise. Averaging values across the entire tumor is the only reliable method of assessment for small tumors.

This study was also limited by the small number of subjects, which was due primarily to the rare nature of ocular melanoma. The data show that the MRI technique is feasible and technically robust, and the preliminary results of an association with monosomy 3 also suggest a clinical role for the technique in evaluating ocular melanoma. Ultimately, our results are hypothesis generating, and larger cohorts will be required to establish the potential significance of the correlation found in this study. The nonsignificant trends toward lower ADC and higher v_p in the setting of monosomy 3 may ultimately prove significant with larger numbers of patients. If validated with a larger group of patients, we propose that mp-MRI could be used in conjunction with fine-needle aspiration to determine chromosome 3 status. The mp-MRI technique could also be applied to other tumors in the head and neck that demonstrate heterogeneous biological behavior.

Conclusions

Multiparametric MRI including quantitative DCE perfusion imaging and artifact-reducing multishot EPI DWI is technically feasible for imaging ocular tumors, despite challenges of susceptibility artifact and eye motion. Further study may show the utility of this technique for risk stratification in uveal melanoma through predicting monosomy 3 and may also show utility in characterizing other tumors.

Ethical standards and patient consent We declare that all human and animal studies have been approved by the UCLA Institutional Review Board and the UCLA Jonsson Comprehensive Cancer Center, and have therefore been performed in accordance with the ethical standards laid down in the 1964 Declaration of Helsinki and its later amendments. Patient consent was waived for the use of patient records in this research study.

Conflict of interest We declare that we have no conflict of interest.

References

1. Damato B (2000) Current management of uveal melanoma. Ophthalmic Physiol Opt 20:S8–S9
2. Chang MY, Rao NP, Burgess BL, Johnson L, McCannel TA (2013) Heterogeneity of monosomy 3 in fine needle aspiration biopsy of choroidal melanoma. Mol Vis 19:1892–1900

3. Stroszczynski C, Hosten N, Bornfeld N et al (1998) Choroidal hemangioma: MR findings and differentiation from uveal melanoma. AJNR Am J Neuroradiol 19:1441–1447
4. Erb-Eigner K, Willerding G, Taupitz M et al (2013) Diffusion-weighted imaging of ocular melanoma. Invest Radiol 48:702–707. doi:10.1097/RLI.0b013e31828eea67
5. Sepahdari AR, Kapur R, Aakalu VK, Villablanca JP, Mafee MF (2012) Diffusion-weighted imaging of malignant ocular masses: initial results and directions for further study. AJNR Am J Neuroradiol 33:314–319. doi:10.3174/ajnr.A2747
6. Rosset A, Spadola L, Ratib O (2004) OsiriX: an open-source software for navigating in multidimensional DICOM images. J Digit Imaging 17:205–216. doi:10.1007/s10278-004-1014-6
7. Ishimori Y, Kimura H, Uematsu H, Matsuda H, Matsuda T, Itoh H (2003) Dynamic T1 estimation of brain tumors using double-echo dynamic MR imaging. J Magn Reson Imaging 18:113–120. doi:10.1002/jmri.10331
8. Vonken EJ, van Osch MJ, Bakker CJ, Viergever MA (1999) Measurement of cerebral perfusion with dual-echo multi-slice quantitative dynamic susceptibility contrast MRI. J Magn Reson Imaging 10:109–117
9. Tofts P, Kermode A (1991) Measurement of the blood-brain barrier permeability and leakage space using dynamic MR imaging. 1. Fundamental concepts. Magn Reson Med 17:357–67
10. Tofts PS, Brix G, Buckley DL et al (1999) Estimating kinetic parameters from dynamic contrast-enhanced T(1)-weighted MRI of a diffusable tracer: standardized quantities and symbols. J Magn Reson Imaging 10:223–232
11. Cramer SP, Simonsen H, Frederiksen JL, Rostrup E, Larrson HBW (2013) Abnormal blood–brain barrier permeability in normal appearing white matter in multiple sclerosis investigated by MRI. Neuroimage Clin 4:182–189. doi:10.1016/j.nicl.2013.12.001
12. de Graaf P, Pouwels PJW, Rodjan F et al (2012) Single-shot turbo spin-echo diffusion-weighted imaging for retinoblastoma: initial experience. AJNR Am J Neuroradiol 33:110–118. doi:10.3174/ajnr.A2729
13. Pulido JS, Campeau NG, Klotz E et al (2008) Correlation of histological findings from a large ciliochoroidal melanoma with CT perfusion and 3T MRI dynamic enhancement studies. Clin Ophthalmol 2:275–281
14. Daftari IK, Aghaian E, O'Brien JM, Dillon WP, Phillips TL (2005) 3D MRI-based tumor delineation of ocular melanoma and its comparison with conventional techniques. Med Phys 32:3355–3362
15. Foti PV, Farina R, Coronella M et al (2015) Diffusion-weighted magnetic resonance imaging for predicting and detecting the response of ocular melanoma to proton beam therapy: initial results. Radiol Med. doi:10.1007/s11547-014-0488-7
16. Yuan Y, Kuai XP, Chen XS, Tao XF (2013) Assessment of dynamic contrast-enhanced magnetic resonance imaging in the differentiation of malignant from benign orbital masses. Eur J Radiol 82:1506–1511. doi:10.1016/j.ejrad.2013.03.001
17. Prescher G, Bornfeld N, Hirche H, Horsthemke B, Jockel KH, Becher R (1996) Prognostic implications of monosomy 3 in uveal melanoma. Lancet 347:1222–1225
18. Chang SH, Worley LA, Onken MD, Harbour JW (2008) Prognostic biomarkers in uveal melanoma: evidence for a stem cell-like phenotype associated with metastasis. Melanoma Res 18:191–200. doi:10.1097/CMR.0b013e3283005270
19. Mouriaux F, Sanschagrin F, Diorio C et al (2014) Increased HIF-1α expression correlates with cell proliferation and vascular markers CD31 and VEGF-A in uveal melanoma. Invest Ophthalmol Vis Sci 55:1277–1283. doi:10.1167/iovs.13-13345
20. Sheidow TG, Hooper PL, Crukley C, Young J, Heathcote JG (2000) Expression of vascular endothelial growth factor in uveal melanoma and its correlation with metastasis. Br J Ophthalmol 84:750–756
21. Sourbron SP, Buckley DL (2011) On the scope and interpretation of the Tofts models for DCE-MRI. Magn Reson Med 66:735–745. doi:10.1002/mrm.22861
22. Koh TS, Bisdas S, Koh DM, Thng CH (2011) Fundamentals of tracer kinetics for dynamic contrast-enhanced MRI. J Magn Reson Imaging 34:1262–1276. doi:10.1002/jmri.22795
23. Jain R (2013) Measurements of tumor vascular leakiness using DCE in brain tumors: clinical applications. NMR Biomed 26:1042–1049. doi:10.1002/nbm.2994